Towards the Zeolitization of Bauxite: Thermal Behaviour of Gibbsite in High-Alumina-Ghanaian Bauxite.

B. Kwakye-Awuah[1 *], E. Von-Kiti[1], I. Nkrumah[1], and C. Williams[3]

[1] Department of Physics (Materials Science Group), KNUST, Kumasi Ghana. Email:

[3] Research Centre in Applied Sciences, University of Wolverhampton, WV1 1LY, United Kingdom

Abstract

Bauxite samples from Awaso mines in Ghana were heated at 100, 300, 500, 800 and 1000 ^{o}C and changes in the $Al_2O_3.H_2O$ phase/composition were investigated using X-ray diffraction (XRD), scanning electron microscopy (SEM), energy dispersive X-ray analysis (EDX), Fourier transformed infrared spectroscopy (FTIR) and particle size analysis. The thermal behaviour of bauxite with time was monitored by Thermogravimetric analysis. The results obtained showed that heating bauxite at 100 ^{o}C is enough to obtain the sodalite structure needed for the zeolitization of bauxite. Heating the bauxite at higher temperatures resulted in the loss of the alumina composition as a result of decomposition of metal carbonates to metal oxides and subsequently the formation of a metal aluminosilicate. The particles size decreased with temperature with average particle size distribution ranging from 8 – 10 µm and 15.5 – 42 µm in the un-heated and treated bauxite respectively.

Keywords: Bauxite, thermal, gibbsite, characterization, zeolite

1. Introduction

Bauxite has been found to be major source of aluminium in our industrial world. It contains alumina (Al_2O_3), silica (SiO_2), Iron (Fe_2O_3) and titanium (TiO_2) and balanced water as the major constituents [8, 10, 13]. The major aluminium bearing mineral phases in bauxite include gibbsite, boehmite and diaspore. Other commonly observed phases include, kaolinites, quartz, goethites, kyanites and hematites. The percentage composition of the aluminium bearing phases in bauxite varies with location and history of formation [8, 10, 14]. For example, Mediterranean type bauxite consists mostly of the boehmite whilst thermal action or low-grade metamorphism favours diaspore formation [14]. Alumina refineries extract pure alumina from bauxite by dissolution in hot caustic soda followed by purification and precipitation of alumina powder which is aluminium oxide (Al_2O_3). During the extraction stage an insoluble sodium aluminosilicate ($NaAlSiO_3$) is produced and precipitated [1, 3, 6, 8, 12, 14]. The precipitated sodium aluminosilicate if modified can be transformed into a more important mineral called zeolite. Zeolites are hydrated crystalline aluminosilicates consisting of

IJERT

pores and cavities that allow ion exchange and reversible dehydration [4, 5]. The central atom consists of either aluminium or silicon that is bonded with oxygen at the corners of tetrahedra and regularly arranged such that channels form [5]. Zeolites have very wide applications from catalysis to ion exchange, from water softening to odour control, from solar heating to refrigeration as well as antimicrobial agents. There are about 40 naturally occurring zeolites and 160 synthetic ones. Depending on the Si/Al ratio the zeolite is used in a particular application. Whilst natural zeolites are cheaper compared with synthetic ones, synthesized zeolites are purer and have the added advantage of modifying the structural content during synthesis to suit a particular application [4,5]. Nevertheless cost benefit of using natural zeolites in addition to the benefit to the environment far outweighs the benefits of using synthetic zeolites. The study of the thermal transformations of aluminium (oxy) hydroxides has resulted in many contradictory findings. Much of this is probably related to the experimental techniques and conditions used to determine these thermal transformations. To date, little have been studied regarding the potential use of the aluminosilicate. The main aim of this research is to transform low grade bauxite from Awaso Mines in Ghana to high-grade, more useful zeolites that can be used to remove heavy metals such as arsenic, lead, manganese among others in mining wastewater in order for it to be drinkable. To achieve this aim, the bauxite phases need to be investigated when thermally treated. This will help understand the kinetics and dynamics of the zeolitization process and the resultant zeolite type that will be produced.

2. Materials and Methods

2.1 Materials and Samples Preparation

The raw bauxite ore was collected from Awaso in the Western region of Ghana. The ore was washed, crushed and milled using a Thomas ball mill machine. The milled sample was passed through a 75 µm sieve to obtain a particle size of at most 75 µm. 75 µm was used because it has been accepted as the boundary between coarse grains and fine grains according to the American Society for Testing and Materials [ASTM E-11-70 (1995)] and British [BS 410 (1986)] standard sieve sizes. 75 µm sieve, grinder, crucibles (Teflon bowls), digital balance and marker were obtained from the Material Engineering laboratory, KNUST. Electric furnace was obtained from the Department of Physics, KNUST.

IJERT

2.2 Thermal Treatment

10 g portion of the grounded bauxite were heated at 100 ^{o}C (A), 300 ^{o}C (B), 500 ^{o}C (C) 800 ^{o}C (D) and 1000 ^{o}C (E). At the end of the heating time, each sample was quenched in air and allowed to cool overnight. The heated samples after cooling were analyzed by XRD, SEM/EDX, FTIR and particle size analysis. The Table 1 gives a summary of the heat treatments that were performed for the bauxite samples.

Table 1: Summary of thermal treatment procedures for the Awaso bauxite

Samples	Heating time (hr)	Temperature (°C)
Un-heated bauxite	-	-
Sample A	1	100
Sample B	2	300
Sample C	3	500
Sample D	3	800
Sample E	3	1000

2.3 Characterization techniques

To confirm the crystal structure and the composition of the synthesized zeolite, it was essential to characterize the zeolite. The X-ray diifraction XRD) pattern of the un-heated and heated bauxite which gives a measure of phase purity were recorded were recorded on Empyrean X-ray powder diffractometer over 2θ range of 3^o to 70^o (PANalytical, UK Ltd, Cambridge). The diffractometer was equipped with a graphite monochromated $Cu\ K_\alpha$ radiation source (8987 eV; $\lambda = 1.5418\ Å$). Data processing was carried out using High Score Plus software with a search/match facility and an ICDD database on a DEC Microvax Minicomputer interfaced to the diffractometer. The surface morphology of the un-heated and heated bauxite as well as the elemental composition was examined by scanning electron microscopy (SEM) using a Zeiss EVO 50 equipped with energy dispersive X-ray spectrometer (EDX) (Zeiss, UK). Aluminium stubs were prepared prior to the analysis with an adhesive coating. The samples were sprinkled on the stubs. Where necessary, the samples were gold-coated using an Emscope SC500 Sputter coater to reduce static charging. Electron micrographs were obtained at various magnifications. Particle size distribution per unit volume was analyzed using a Mastersizer long bed analyzer (Malvern Instruments, UK). Samples of the un-heated and heated bauxite were taken for particle size analysis. Before measurements were made, the laser lenses were aligned in a straight line. Settings were set to obscuration value of 0.2. After steady conditions, 0.1 mg of each sample was loaded into an MSX 15 sample handling unit that uses the mechanical action of stirring to ensure that the zeolite particles did not flocculate. Sodium Amalgam was then added to disperse adhering particles. Measurements were then recorded on a computer connected to the instrument. The vibrational properties were investigated by Fourier transformed infrared spectrometry (FTIR). Measurements were done using 100 scans at 4 cm^{-1} resolution, units of log (1/R) (absorbance), over the mid-infrared mid-IR region of 1200-400 cm^{-1}. An air background spectrum was collected at the start of the sample analysis. A small sample of each of the un-heated or heated bauxite was centred on the ZnSe plate to ensure that it covered the entire crystal surface, and a pressure clamp was used to apply pressure on the sample. The zeolite samples were analyzed three times for three different samples. A background spectrum was measured before samples were scanned to compensate for atmospheric conditions around the FT-IR instrument. Thermogravimetric analysis (TG –DTA) was performed using a Perkin Elmer TGA 7 (Perkin Elmer, UK) with differential thermal analysis. The study was carried out by heating at 10 °C /min heating rate starting from room temperature, with sensitivity of 0.2 mV in atmospheric conditions, and the changes in the sample due to heating were observed. The temperature range for the analysis was 50 ^{o}C to 800 ^{o}C.

IJERT

3. Results and discussions

3.1 Characterization results

Results from the EDX analysis (Table 2) showed that bauxite was found to contain high amount of alumina as compared to the other compounds; silicon oxide, titanium oxide and iron oxide.

The alumina/silica ratio for each heating time and temperature with respect to their atomic weight were 49.3:1 in un-heated bauxite, 116:1 for bauxite heated at 100 ^{o}C, 152:1 for bauxite heated at 300 ^{0}C and 17.6:1 at 500 ^{o}C. The alumina/silica ratio however, decreased (11.7:1) at 800 ^{o}C and further decreased to 15.8:1 at 1000 ^{o}C. The associated spectrum of elemental composition is presented in Figure. 1: Results from the XRD analysis indicated changes in the phases of the bauxite at the various heat treatments are shown in Figure 2. Rietveld analysis (not shown) showed that the main composition of the un-heated bauxite was almost gibbsite (Table 3). After heating the bauxite at 100 ^{o}C sodalite phase appeared. Sodalite is a mineral consisting of aluminosilicate framework with SiO_4 and AlO_4 tetrahedra present in approximately equal numbers having rings of either four-fold or six-fold. It has a cubic structure with crystallographic parameters: $P-43n\ (No.218), a = 8.8820, \text{Å}, a = b = g = 90.0, Z = 1$ [10]. The formation of the sodalite structure gives an insight of the zeolitization process since many zeolite structures are based on the formation of sodalite cages. When heated above 100 ^{o}C, the sodalite structure was converted to Gibbsite (at 300 ^{o}C) and remained same up at 500, 800 and 1000 ^{o}C. However, most of the gibbsite peaks disappeared at temperatures above 500 ^{o}C. This may be due to the fact that hematite and rutile were the dominant phases (Figure 2). Thermal treatment kinetics graph is presented in Figure 3. Weight loss of ≈ 1.26 % of its total weight occurred between 24 and 50 ^{o}C showing that the bauxite was highly crystalline and that the proportion of absorbed water is very small. A small weight loss of ≈ 1 % the temperature range of 30 – 100 ^{o}C can be attributed to loss of water on the surface of the bauxite. This is the initial step of the decomposition of bauxite which involves the diffusion of protons and the reaction with hydroxyl ions to form water [7, 8, 13, 14, 22]. This process removes the binding forces between subsequent units in the gibbsite structure and causes changes in the chemical composition and density [6, 10, 16, 17]. The more pronounced weight loss at 330 ^{o}C with a mass change of ≈ 24.70 % could be attributed to the loss of chemically bound water in the bauxite. The lost chemically bound water could be mainly attributed to the decomposition of gibbsite ($Al(OH)_3$) to alumina (Al_2O_3) and H_2O as shown by the XRD (Figure 2) and FTIR spectra (Figure 6). The loss in peaks in both XRD and FTIR spectra indicate that the lost chemically bound water reacted with sodium, calcium or magnesium oxide to form trisodium, trimagnesium or tricalcium aluminate [9]. The endotherms around 410 and 534 ^{o}C could be attributed to the release of CO_2 according to the equations (using calcium for example) [2, 3, 4, 7, 8, 19]:

$$CaCO_3 \rightarrow CaO + CO_2 \qquad \text{(R1)}$$

$$3CaO + Al_2O_3 \rightarrow Ca_3Al_2O_6 \qquad \text{(R2)}$$

The calcium oxide may also have reacted with the alumina and silica as presented by the equation:

$$2CaO + 2Al_2O_3 + SiO_2 \rightarrow 2Ca_2Al_2SiO_7 \qquad \text{(R3)}$$

Thus the formation of the metal aluminosilicates was responsible for the loss of peaks in both the XRD and FTIR

IJERT

spectra. SEM images (Figure 4) confirmed the crystal morphology of the bauxite samples heated. The particles are very fine in size (5 – 20 µm) with irregular shapes. The white crystal obtained at 500, 800 and 1000 ^{o}C showed the dominance of hematite phase at the expense of alumina phase. This is because the alumina phase is likely to have formed the metal aluminosilicate resulting in their disappearance. Such changes in phase/composition confirm in both the un-heated bauxite and the thermally treated bauxite is consistent with previous report [10, 11, 17, 18]. Modal size distribution obtained for the un-heated bauxite was 22.9 µm (Figure 5). On heating the bauxite to 100 ^{o}C the modal distribution was reduced to 26. 3 µm. This is likely to be attributed to the formation of the sodalite structure which opened the structure as result of the formation of pores or voids in the structure. When heated to 300 ^{o}C the mode decreased to 17. 4 µm. This may be an indication of the loss of the chemically bound water in the bauxite. The mode increased to 19.9 µm on heating the bauxite to 300 ^{o}C. This is attributed to the formation of the metal aluminosilicate. Heating the bauxite at 800 and 1000 ^{o}C resulted in a in the modal distribution of 19.9 and 10.2 µm respectively. FIG. VI(a-f) shows the FTIR spectrum of un-heated bauxite and bauxite that of bauxite heated at 100 ^{o}C, 300 ^{o}C, 500 ^{o}C, 800 ^{o}C and 1000 ^{o}C. For sample of the un-heated bauxite, peaks occurred at 3618, 3524, 3452, 3392, 3370, 1017, 966, 730, 662, 555, 477, 448 and 407 cm-^{1}. The peaks at 3618, 3524, 3452, 3392, 3370 cm^{-1} is assigned to the OH stretching of gibbsite [3, 10, 11, 14, 15]. These peaks disappeared on heating the bauxite from 100 ^{o}C. The OH bending peak at 1017 cm^{-1} which is the strongest in the un-heated bauxite broadened and shifted to a lower wavenumber (939 cm^{-1}) at 100 ^{o}C, disappeared at 300, 500 and 800 ^{o}C and re-appeared (920 cm^{-1}) with moderate strength at 1000 ^{o}C. The peak at 939 cm^{-1} may be may be attributed to the formation sodalite structure at 100 ^{o}C [11, 12, 18, 20, 21]. The disappearance of the peaks at higher temperatures ($T > 500°C$) corresponds with the endotherms around 509 and 534 ^{o}C in the DTA pattern [10, 13]. The metallic vibrations which are assigned to peaks at 1650 cm^{-1} was not observed.

4. Conclusion

Bauxite tailings from Awaso mines in Ghana has been characterized and thermally investigated at different temperatures. Heating the bauxite at 100 ^{o}C was enough for the sodalite structure which is the basic structure of most zeolites. Heating at higher temperatures ($T > 300°C$) resulted in the loss of peaks in both XRD and FTIR spectra and a resulting endotherms in the TG-DTA curve. Heating the bauxite at higher temperatures resulted in the loss of the alumina composition as a result of decomposition of metal carbonates to metal oxides and subsequently the formation of a metal aluminosilicate. The particles size decreased with temperature with average particle size distribution ranging from 8 – 10 µm to 15.5 – 42 µm in the un-heated and treated bauxite respectively.

IJERT

5. References

[1] A. Alp and A. O. Aydin: Effect of Alkaline Additives on the Thermal Properties of Bauxite. *J. Therm Anal*. **53**, (1998), 141 – 49.

[2] A. Hind, S. Bhargava and S. Grocott: The surface chemistry of Bayer process solids: a review. *Colloid Surfaces A: Physicochem. Eng. Aspects*.**146**, (1999), 359-374.

[3]A. Pehliva, A. O. Aydin and A. Alp: Alumina extraction from low-grade diasporic bauxite by pyro-hydro metallurgical process. *SAÜ. Fen Bilimleri Dergisi*. **16**(2), (2002), 92 – 98.

[4] A. Aronne, S. Esposito and P. Pernice: FTIR and DTA study of lanthanum aluminosilicate glasses. *Mater. Chem. Phys*.51, (1997), 163.

[5] B. Kwakye-Awuah, I. Radecka, M. A. Kenward and C. D. Williams: Production of silver-doped analcime by isomorphous substitution technique. *J. Chem Tehcnol Biotechnol*.**83**(9), (2008), 1255 – 1260.

[6] C. Colombo and A. Violante: Effect of time and temperature on the chemical composition and crystallization of mixed iron and aluminum species. *Clays Clay Miner*. **44** (1), (1996), 113.

[7] D. Dodoo-Arhin, D. S. Konadu, E. Annan, F. P Buabeng, A. Yaya, and B. Agyei-Tuffour: Fabrication and Characterisation of Ghanaian Bauxite Red Mud-Clay Composite Bricks for Construction Applications. *Amer. J. Mater. Sci*. **3**(5), (2013), 110 – 119.

[8] E. Annan, B. Agyei-Tuffour, L. N. W. Damoah, D. S. Konadu and B. Mensah. Physico-mechanical properties of bauxite residue-clay bricks, *ARPN J. Eng. Appl. Sci*.**7**(12), (2012), 1587 – 1594.

[9] J. Pascual, F. A. Corpas, J. López-Beceiro, M. Benítez-Guerrero and R. Artiaga: Thermal Characterization of a Spanish Red mud. *J. Therm Anal Calorim*.**96**(2), (2009), 407 – 412.

[10] J. T. Kloprogge, H. D. Ruan and R. L. Frost: Thermal decomposition of bauxite minerals: infrared emission spectroscopy of gibbsite, boehmite and diaspore. *J. Mater. Sci*.**37**(6), (2002), 1121 – 1129.

[11] M. G. Sujana and S. Anand: Flouride removal studies from contaminated ground water by using bauxite. *Desalination*.**267**, (2011), 222 – 227.

[12] M. Gräfe, G. Power and C. Klauber: Bauxite residue issues: III. alkalinity and associated chemistry. *Hydrometallurgy*.**108**, (2011), 60 – 79.

[13] M. L. Costa: Lenterization as the the major deposit of ore. *Explor. Min. Geol*. **6**, (1997), 79 – 104.

[14] R. L. Frost, J. T. Kloprogge , S. C. Russell and J. L. Szetu: Vibrational *spectroscopy* and dehydroxylation of aluminum (Oxo)hydroxides: gibbsite. *Appl. Spectrosc*. **53**, (1999), 423.

[15] S. Meseaguer, F. Pardo, M. M. Jordan, T. Sanfeliu and I. Gonzalez: Ceramic behaviour of five Chilean clays which can be used in Manufacture of ceramic tile bodies. *Appl. Clay Sci*. **47**, (2010), 372 – 377.

[16] S. Snigdha and V. S. Batra: Catalytic applications of red mud, an aluminium

IJERT

industry waste: A review. *Appl. Cat. B, Environ*. **81**, (2008), 64 – 77.

[17] S. Srikanth, A. K. Ray, A. Bandopadhyay, B. Ravikumar and J. Animesh:. Phase constitution during sintering of red mud and red mud-fly ash mixtures. *J. Am. Ceram. Soc*. **88**(9), (2005), 2396 – 2401.

[18] T. Hiemstra and W. H. Van Riemsdijk: Flouride adsorption on goethite in relation to different types of surface sites. *J. Colloid Interf. Sci*.**225**, (2000), 94 – 104.

[19] V. J. Ingram-Jones, R. C. T. Slade, T. W. Davies, J. C. Southern and D. Salvador: Dehydroxylation sequences of gibbsite and boehmite: study of differences between soak and flash calcination and of particle-size effects. *J. Mater. Chem*. **6**, (1996), 73.

[20] V. M. Sglavo, R. Campostrini, S. Maurina, G. Carturan, M. Monagheddu, G. Budroni and G. Cocco: Bauxite red mud in the ceramic industry. Part 1: Thermal Behaviour. *J. Eur. Ceram. Soc*. **20**(3), (2000), 235 – 244.

[21] X. Liu, N. Zhang, H. Sun, J. Zhang, and L. Li: Structural investigation relating to the cementitious activity of bauxite residue-red mud. *Cement Concrete Res*. **41**(8), (2011), 847 – 853.

[22] Ž. D. Živković, N. D. Štrbac and J. Šesták: Thermal decomposition of low-grade high-silicon boehmite bauxite *Thermochimica Acta*. **233**(1), (1994), 97 – 105.

IJERT

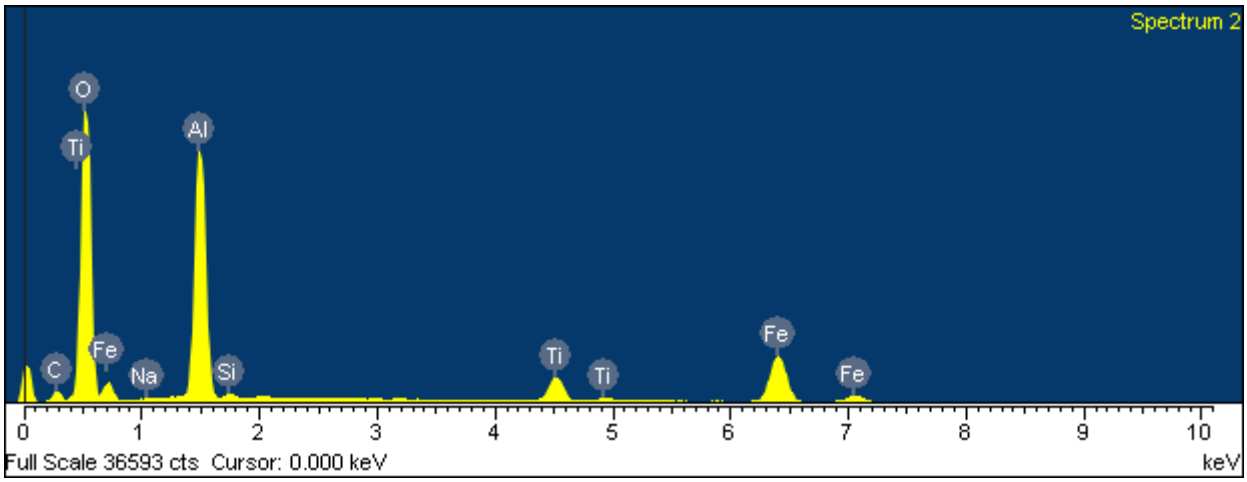

Figure 1: EDX spectrum of bauxite showing the major elements in the bauxite

Table 2: Elemental composition of bauxite and that of bauxite heated at (a): 100 ^{o}C, (b): 300 ^{o}C, (c) 500 ^{o}C, (d): 800 ^{o}C and (E): 1000 ^{o}C

Temperature (^{o}C)	Elemental composition (%)						
	Al_2O_3	SiO_2	TiO_2	FeO_3	Na_2O	CaO	L.O.I.
Un-heated	69.30	1.41	1.67	3.42	1.03	0.08	23.09
100 ^{o}C	69.59	0.60	0.53	4.183	1.01	0.09	24.00
300 ^{o}C	69.96	0.46	1.14	3.22	1.02	0.08	24.12
500 ^{o}C	65.28	0.37	0.38	2.85	1.02	0.08	30.02
800 ^{o}C	62.06	0.53	1.10	5.63	1.01	0.09	29.58
1000 ^{o}C	59.97	3.79	0.71	4.30	1.03	0.06	30.14

IJERT

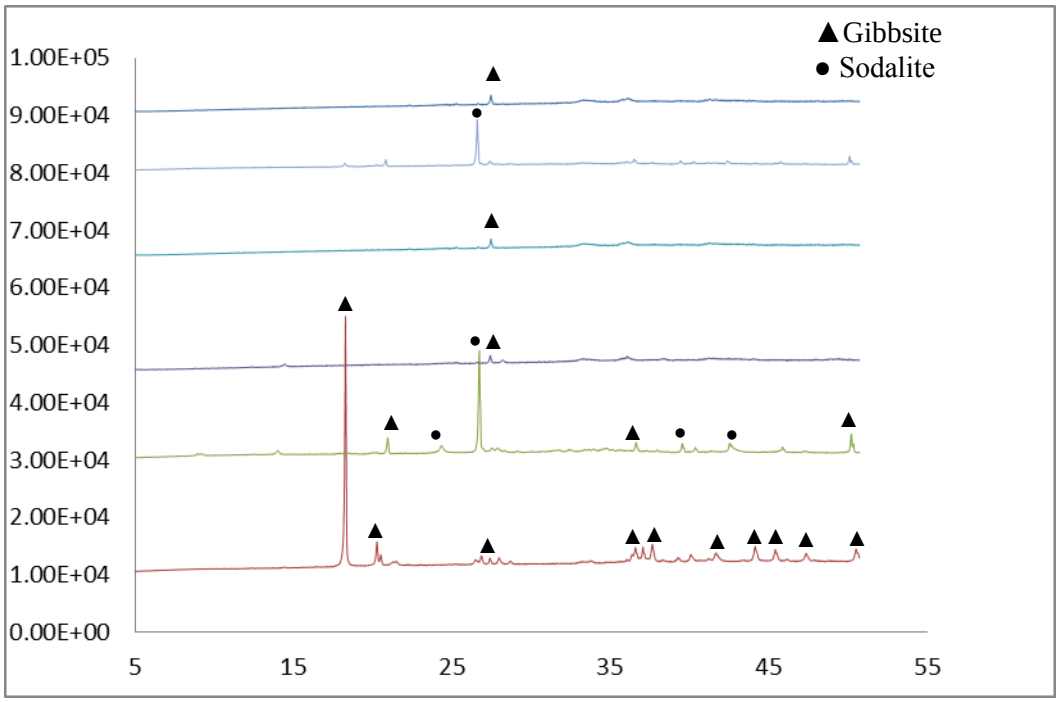

Figure 2: XRD spectrum of (a): unheated bauxite and for bauxite heated at (b): 100 ^{o}C, (c): 300 ^{o}C, (d): 500 ^{o}C (e): 800 ^{o}C and (f): 1000 ^{o}C

IJERT

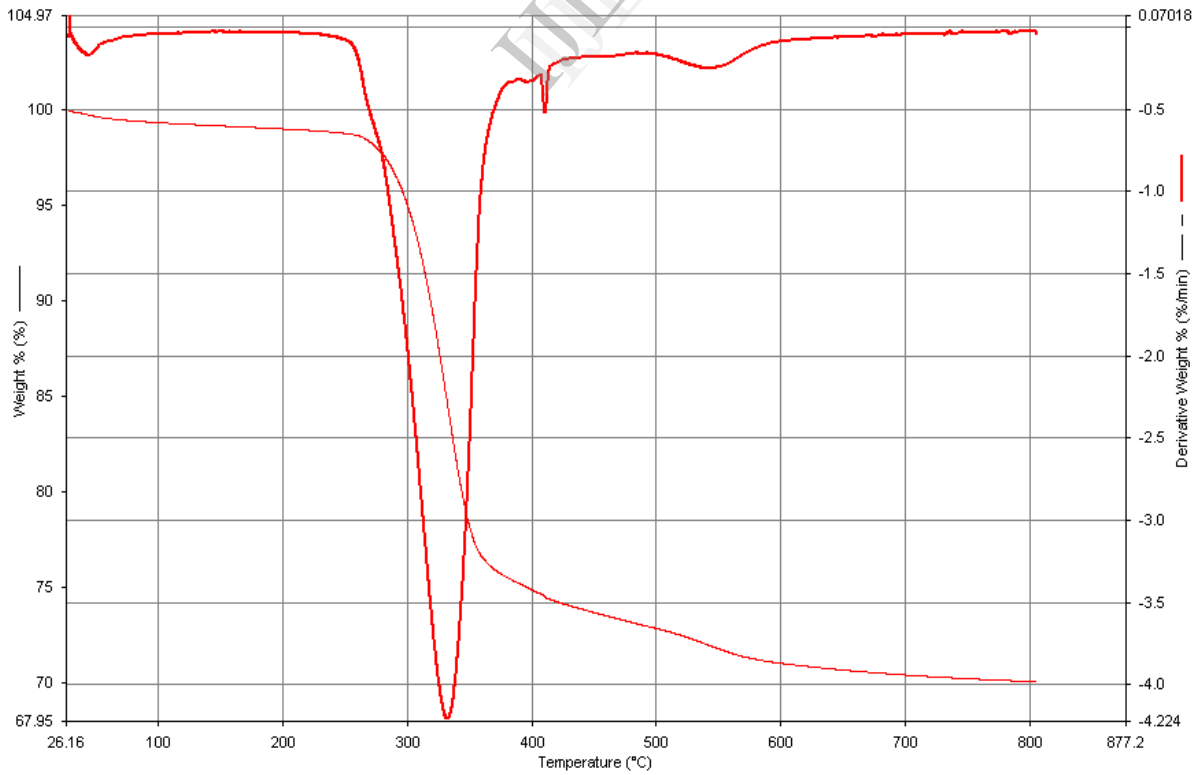

Figure 3: TGA with DTA curves of bauxite within the temperature range of 24 ^{o}C and 800 ^{o}C

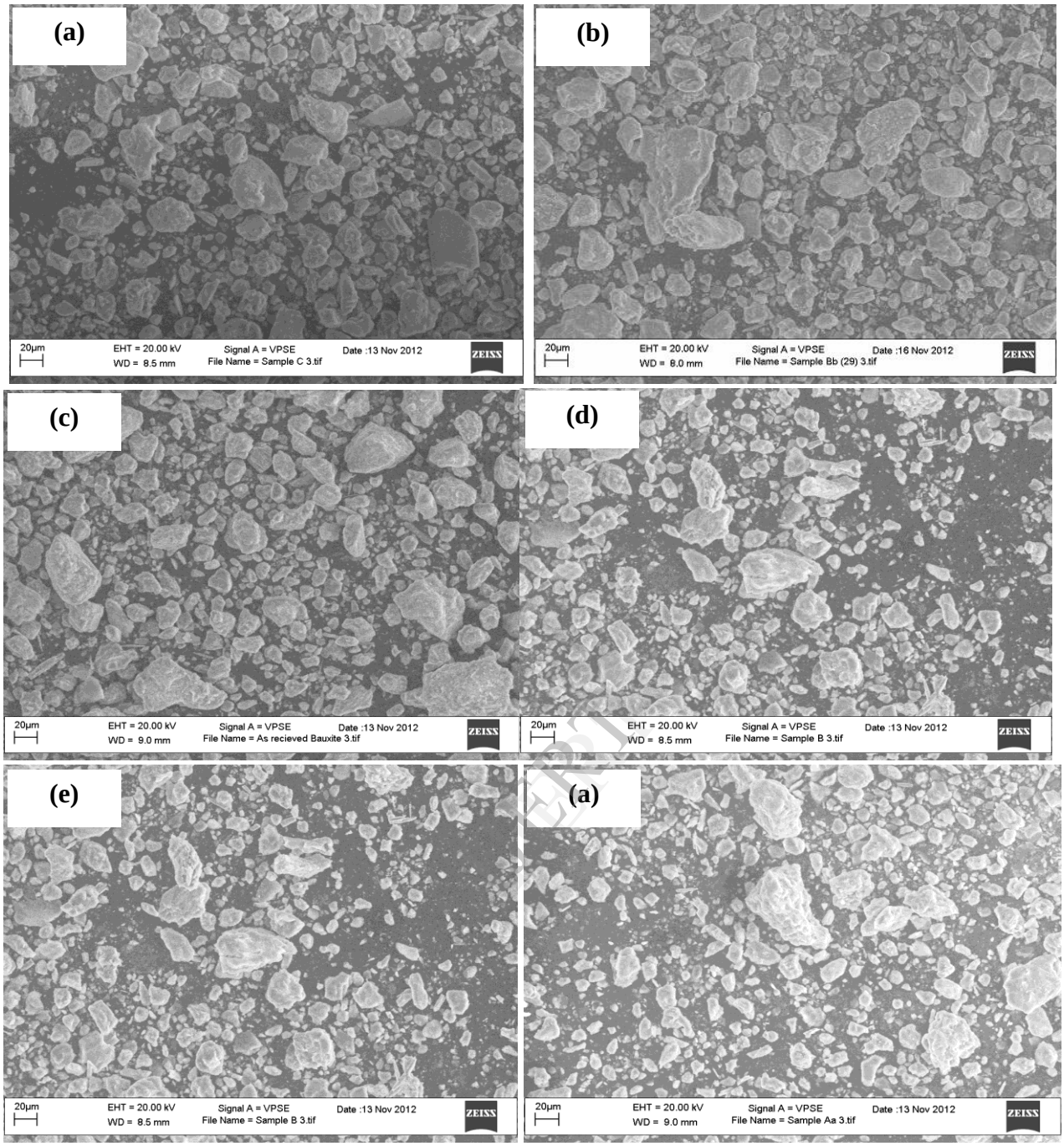

Figure 4: Scanning electron micrograph of (a): unheated bauxite and for bauxite heated at (b): 100 ^{o}C, (c): 300 ^{o}C, (d): 500 ^{o}C, (e): 800 ^{o}C and (f): 1000 ^{o}C

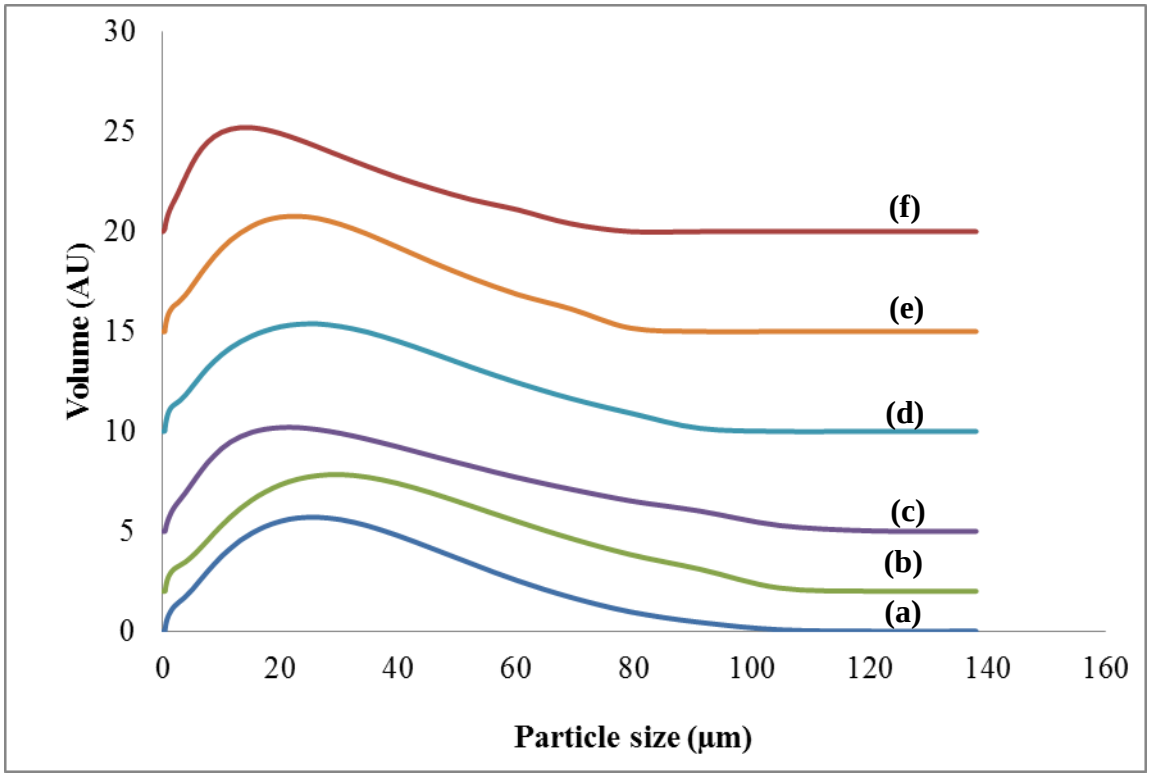

Figure 5: Particle size distribution of bauxite (a) and bauxite heated at (b) 100 ^{o}C, (c): 300 ^{o}C, (d): 500 ^{o}C, (e): 800 ^{o}C and (f): 1000 ^{o}C.

IJERT

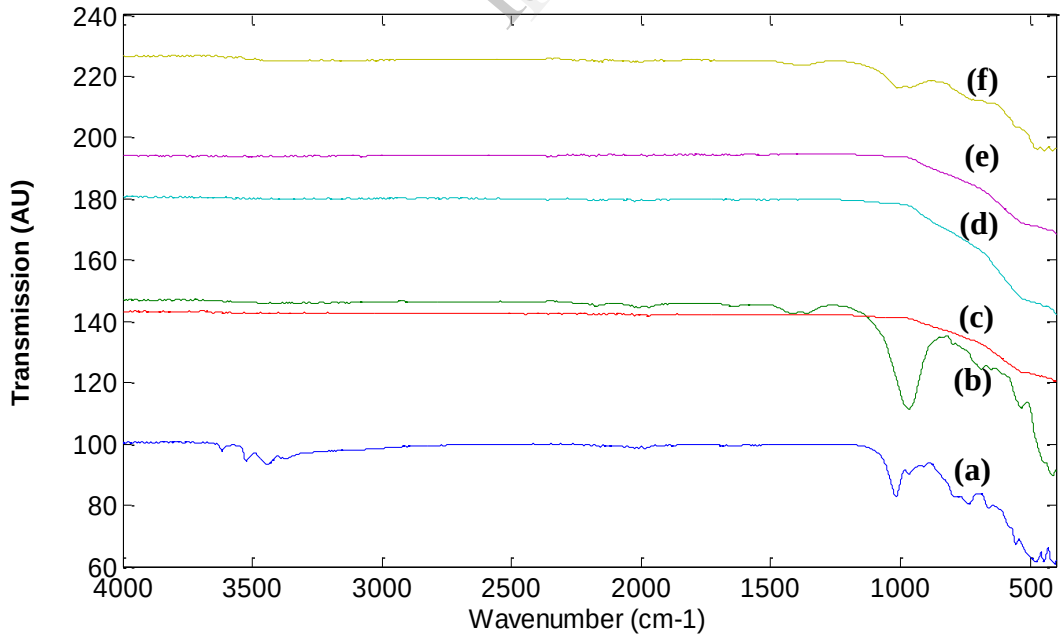

Figure 6: FTIR spectrum of (a): un-heated bauxite and for bauxite heated at (b): 100 ^{o}C, (c): 300 ^{o}C, (d): 500 ^{o}C, (e): 800 ^{o}C and (f): 1000 ^{o}C.